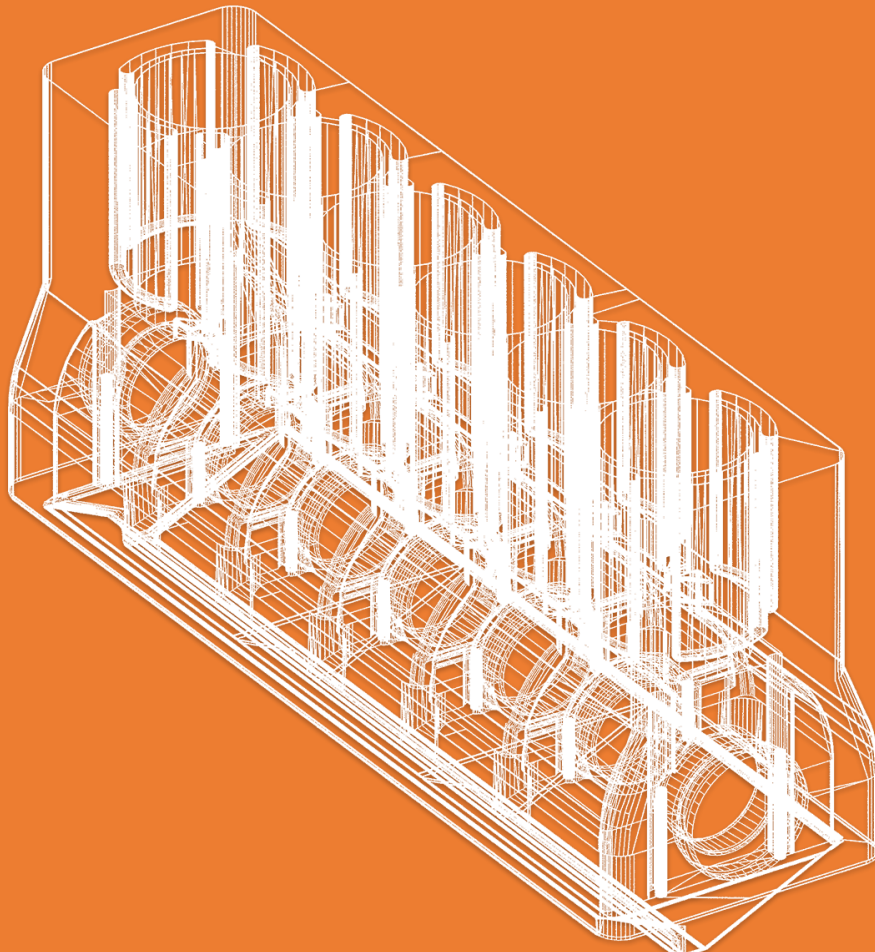


Vibration study of an inline-six internal combustion engine



Authors

Alexis Cariou
Lorenzo Clerici
Dario D'Orsi
Pietro Musso
Abdelhkim Nakiata
Giacomo Pirani
Matteo Raggi
Elia Zamperoni

Table of contents

1. Abstract	3
2. Theoretical development.....	4
2.1. Physical model and aims of the project	4
2.2. Definition of the system's equations.....	5
2.2.1. Kinetic energy	5
2.2.2. Potential energy	6
2.2.3. Inertial forces	8
2.2.4. Final Lagrangian equations.....	10
2.3. Modal analysis	13
2.4. Time response.....	14
2.5. Forces transmitted to the chassis.....	15
2.6. Spectral analysis	16
3. Numerical implementation.....	17
3.1. P.I.E. classes and interactions	17
3.2. Definition of the engine data.....	20
4. Simulation results.....	25
4.1. Static measurements: determination of system parameters	25
4.2. Speed ramp: from idle to limiter	26
4.3. Steady forcing: idle regime	29
4.4. Steady forcing: maximum power regime	32
4.5. Steady forcing: limiter regime	35
4.6. Real engine simulation: maximum power regime	38
4.7. Experimental validation: resonance and error analysis	39
5. Conclusions and final remarks	41
6. References	42
Figures.....	43
Tables.....	43



1. Abstract

This study's objective is the definition of the response of an inline-six engine under the forcing of its own inertial forces, produced by the crank and slider mechanism present in each cylinder of the engine. To do so, a theoretical model of the forcing action and of the engine mounts is developed, and its numerical implementation is performed in MATLAB.

Additionally, in order to further expand the scope of the study and provide tools for future works on the same matter, a parametric and modular system of classes is developed, allowing for studies on any engine characterized by an inline configuration, given a set of arbitrary parameters through a purpose-built graphic user interface.

Finally, testing of the model is carried out both in steady forcing conditions and over speed ramps, highlighting the amplitude and frequency of the response of the system by analysing the time domain and spectra of the resulting signals, both in the case of an ideal engine and of an engine built with real dimensional tolerances.

2. Theoretical development

2.1. Physical model and aims of the project

The simplified physical model consists in a monolithic prismatic rigid body with six degrees of freedom (three displacements and three rotations), mounted on four viscoelastic supports, each made of three orthogonal springs and dampers.

The reference frame has been placed on the engine's center of gravity, with the axis parallel to the block's edges (see Figure 1).

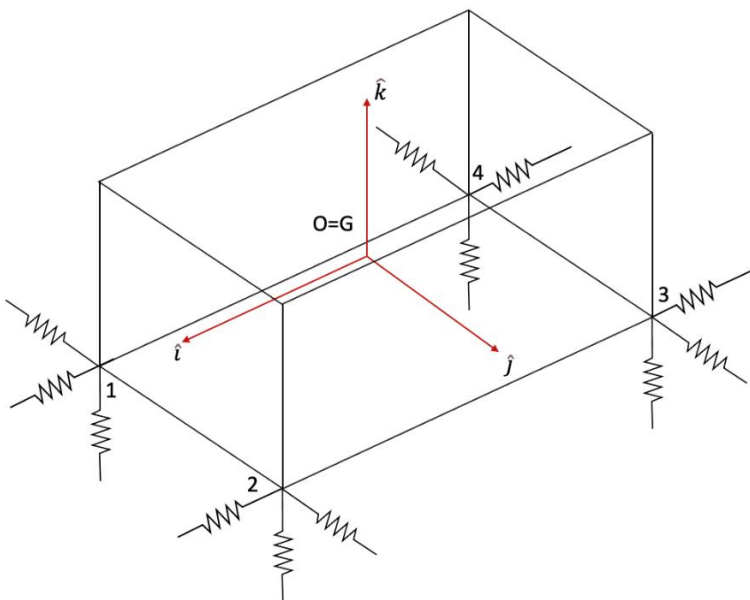


Figure 1 - Simplified Model

2.2. Definition of the system's equations

To model the six degree of freedom system, the Lagrangian approach has been chosen. The equation of motion can therefore be obtained using the following relation:

$$\frac{d}{dt} \left(\frac{\partial T}{\partial \dot{x}_i} \right) - \frac{\partial T}{\partial x_i} + \frac{\partial U}{\partial x_i} = Q_i \quad (1)$$

Where T is the total kinetic energy, U represents the total potential energy, Q is the contribute to the motion given by all the external and non-conservative forces and x is the generalized coordinate chosen to describe the motion of the system.

The non-conservative forces related to the dampers haven't been initially considered in the Lagrange equations, but they have been added later, by assuming a proportional damping.

Since the case study consists of a six DOF model, equation **(1)** gives a system of six differential equations, one for each generalized coordinate x_i .

The six generalized coordinates chosen in order to describe the motion of the system are the following:

- x_G = displacement of the center of mass along \hat{i} ;
- y_G = displacement of the center of mass along \hat{j} ;
- z_G = displacement of the center of mass along \hat{k} ;
- Θ_x = rotation of the engine block around \hat{i} ;
- Θ_y = rotation of the engine block around \hat{j} ;
- Θ_z = rotation of the engine block around \hat{k} ;

According to this reference system, all the terms of the Lagrangian equations have been written.

Hereafter is presented the procedure followed in order to find the kinetic energy, the potential energy, and the forcing vector.

2.2.1. Kinetic energy

The kinetic energy of the system is given by the following equation:

$$T = \frac{1}{2} m(\bar{v}_G)^2 + \frac{1}{2} \bar{\omega} \cdot \mathbb{I}_G \bar{\omega} \quad (2)$$

Where \bar{v}_G is the velocity of the center of mass, $\bar{\omega}$ is the angular velocity of the body and \mathbb{I}_G is the inertia matrix of the body, referred to its center of mass.

\bar{v}_G and $\bar{\omega}$ can be written as:

$$\bar{v}_G = \dot{x}_G \hat{i} + \dot{y}_G \hat{j} + \dot{z}_G \hat{k} \quad (3)$$

$$\bar{\omega} = \dot{\theta}_x \hat{i} + \dot{\theta}_y \hat{j} + \dot{\theta}_z \hat{k} \quad (4)$$

Therefore, the total kinetic energy obtained is:

$$\begin{aligned} T = & \frac{1}{2} m (\dot{x}_g^2 + \dot{y}_g^2 + \dot{z}_g^2) \\ & + \frac{1}{2} \left(I_{11} \dot{\theta}_x^2 + I_{12} \dot{\theta}_x \dot{\theta}_y + I_{13} \dot{\theta}_x \dot{\theta}_z + I_{21} \dot{\theta}_y \dot{\theta}_x + I_{22} \dot{\theta}_y^2 \right. \\ & \left. + I_{23} \dot{\theta}_y \dot{\theta}_z + I_{31} \dot{\theta}_z \dot{\theta}_x + I_{32} \dot{\theta}_z \dot{\theta}_y + I_{33} \dot{\theta}_z^2 \right) \end{aligned} \quad (5)$$

2.2.2. Potential energy

In the formulation of the potential energy term, only dynamic displacements of the springs from their equilibrium point are taken into consideration. This is obviously due to the balancing between the weight of the engine and the static displacement of the springs.

The definition of the displacement of every spring has been handled by considering the displacements along one axis at time.

The adopted procedure is the following (for simplicity, it will be reported only the one along the z axis, characterised by verson \hat{k}):

- The displacement of each spring has been calculated as the algebraic sum of three different displacements.
 - The first one is due to the movement of the centre of mass along \hat{k} .
 - The second one is due to the rotation of the system around \hat{j} .
 - The third one is due to the rotation of the system around \hat{i} .
- The two rotational contributions to the springs' displacements have been considered equal to $d_{ij}\theta_k$, where d_{ij} is the distance of the mounting point from the axis of rotation and θ_k is the angle of rotation. In this expression, sine is simplified under the assumption of small rotations.

Along the z axis \hat{k} , for clarity, they are $d_{xz}\theta_y$ and $d_{yz}\theta_x$ (see Figure 2).

- The elastic potential energy of each spring along \hat{k} has been calculated as:

$$U_{zi} = \frac{1}{2} k_i (\pm z_g \pm d_{xz}\theta_y \pm d_{yz}\theta_x)^2 \quad (6)$$

$i \in \{1, 2, 3, 4\}$

- The total potential energy along \hat{k} can be therefore written as:

$$U_z = \sum_{i=1}^4 U_{zi} \quad (7)$$

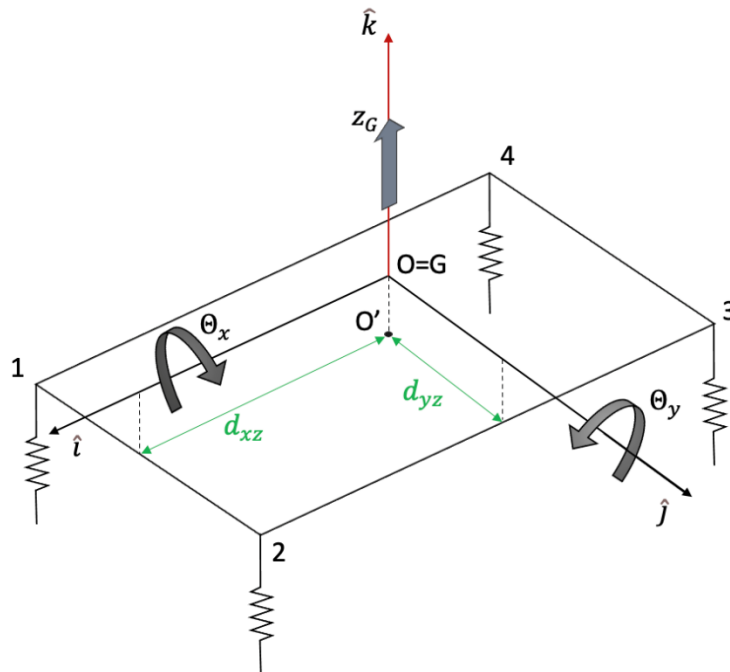


Figure 2 - Calculation of the springs' displacements along the vertical axis

Reorganizing all the terms and extending this procedure to the other two axes, the following equations can be obtained:

$$\begin{aligned} \cdot U_x = & \frac{1}{2}(k_1 + k_2 + k_3 + k_4)(x_g^2 + d_{xz}^2\Theta_y^2 + d_{xy}^2\Theta_z^2) \\ & - (k_1 + k_2 + k_3 + k_4)x_G d_{xz}\Theta_y + (k_1 - k_2 - k_3 + k_4)x_G d_{xy}\Theta_z \\ & + (-k_1 + k_2 + k_3 - k_4)d_{xz}d_{xy}\Theta_y\Theta_z \end{aligned} \quad (8)$$

$$\begin{aligned} \cdot U_y = & \frac{1}{2}(k_1 + k_2 + k_3 + k_4)(y_g^2 + d_{yz}^2\Theta_x^2 + d_{xy}^2\Theta_z^2) \\ & + (k_1 + k_2 + k_3 + k_4)y_G d_{yz}\Theta_x + (k_1 + k_2 - k_3 - k_4)y_G d_{xy}\Theta_z \\ & + (+k_1 + k_2 - k_3 - k_4)d_{yz}d_{xy}\Theta_x\Theta_z \end{aligned} \quad (9)$$

$$\begin{aligned} \cdot U_z = & \frac{1}{2}(k_1 + k_2 + k_3 + k_4)(z_g^2 + d_{yz}^2\Theta_x^2 + d_{xz}^2\Theta_y^2) \\ & + (-k_1 + k_2 + k_3 - k_4)z_g d_{yz}\Theta_x + (-k_1 - k_2 + k_3 + k_4)z_g d_{xz}\Theta_y \\ & + (-k_1 + k_2 + k_3 - k_4)d_{yz}d_{xz}\Theta_x\Theta_y \end{aligned} \quad (10)$$

Finally, the total potential energy of the system is:

$$U = U_x + U_y + U_z \quad (11)$$

2.2.3. Inertial forces

The vibrations of the engine are the result of the inertial forces generated by the movement of the pistons, rods and the cranks due to the combustion. For clarity, the crankshaft of the engine in exam has been placed parallel to \hat{t} .

In order to simplify the problem, the connecting rod has been substituted with two punctual masses m_a and m_b (one in the big end and one in the small end of the rod) and one inertial moment J_0 , following the relation:

$$\begin{cases} m_a = m_{cr} \frac{b}{l} \\ m_b = m_{cr} \frac{a}{l} \\ J_0 = J_{cr} - m_b ab \end{cases} \quad (12)$$

Where m_{cr} is the connecting rod's mass, l the connecting rod's length, J_{cr} the moment of inertia of the connecting rod, and a and b are the distances of the two substitutional masses from the centre of gravity of the connecting rod.

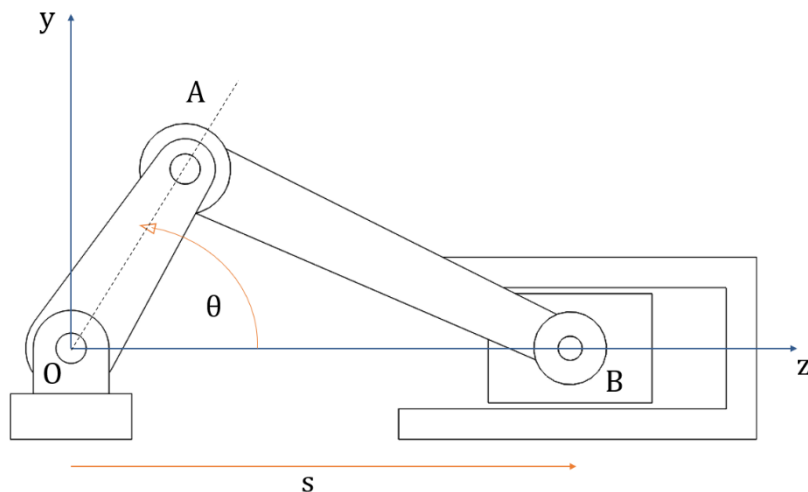


Figure 3 - Model for the inertial forces

It's now possible to define the displacement of the piston as:

$$\bar{s}(\theta) = (r \cos \theta + l \sqrt{1 - (\lambda \sin \theta)^2}) \hat{k} \quad (13)$$

Where r is the crank's length, θ is the crank's angle and λ the ratio between r and l .

By calculating the second derivative of equation (13) we obtain the acceleration of the piston:

$$\ddot{\bar{s}} = -r\omega^2 \left[\cos(\theta) - \frac{r(l^2 - 2l^2 \cos^2 \theta - r^2 \sin^4 \theta)}{(l^2 - r^2 \sin^2 \theta)^{\frac{3}{2}}} \right] \hat{k} \quad (14)$$

The reciprocating inertial force generated by the movement of the piston can be obtained by multiplying its acceleration by its mass and changing the sign:

$$\bar{F}_a = (m_p + m_b)r\omega^2 \left[\cos(\theta) - \frac{r(l^2 - 2l^2 \cos^2 \theta - r^2 \sin^4 \theta)}{(l^2 - r^2 \sin^2 \theta)^{\frac{3}{2}}} \right] \hat{k} \quad (15)$$

The crank, instead, generates a rotating force, of which the module is given by:

$$F_r = (m_{ck}r_G + m_a r)\omega^2 \quad (16)$$

Where m_{ck} is the mass of the crank, and r_G is the distance between the crankshaft and the connecting rod's centre of gravity.

Once F_r is defined, it's possible to decompose it in two reciprocating forces, one vertical and one horizontal, by the following relations:

$$\bar{F}_h = F_r \sin \theta \hat{j} \quad (17)$$

$$\bar{F}_v = F_r \cos \theta \hat{k} \quad (18)$$

The total forcing vector for each cylinder will be therefore:

$$\bar{F}_i = F_r \sin \theta_i \hat{j} + (F_a + F_r \cos \theta_i) \hat{k} \quad (19)$$

$$i \in \{1, 2, 3, 4, 5, 6\}$$

Where θ_i is the crank angle of each piston, which includes the phase shift imposed by the crankshaft design, in this case equal to $\{0, 120, 240, 240, 120, 0\}$.

It's therefore possible to calculate the total forces that excite the engine along \hat{j} and \hat{k} :

$$F_y = \sum \bar{F}_i \cdot \hat{j} \quad (20)$$

$$F_z = \sum \bar{F}_i \cdot \hat{k} \quad (21)$$

It's important to notice that there's no force along the \hat{i} axis.

In addition to the forces, a moment is generated by the rotation of the connecting rod. If γ is the angle of the connecting rod, the following equivalence can be obtained from the mechanism's geometry:

$$\gamma(\theta) = \sin^{-1}(\lambda \sin(\theta)) \quad (22)$$

By deriving twice equation (22) the angular acceleration of the connecting rod can be obtained:

$$\ddot{\gamma}(\theta) = \frac{2\sqrt{2}\lambda(\lambda^2 - 1)\omega^2 \sin(\theta)}{(2 - \lambda^2 + \lambda^2 \cos(2\theta))^{\frac{3}{2}}} \quad (23)$$

The moment for each piston will therefore be:

$$\bar{M}_{cri} = -J_0 \frac{2\sqrt{2}\lambda(\lambda^2 - 1)\omega^2 \sin(\theta_i)}{(2 - \lambda^2 + \lambda^2 \cos(2\theta_i))^{\frac{3}{2}}} \hat{i} \quad (24)$$

Where:

$$J_0 = J_{cr} - m_{cr} \frac{l}{COG_{factor}} \quad (25)$$

$$J_{cr} = \frac{m_{crl}l^2}{12} + m_{cr} \left(\frac{l}{2} - \frac{l}{COG_{factor}} \right)^2 \quad (26)$$

$$COG_{factor} = \frac{l}{l_{COG}} \quad (27)$$

l_{COG} is defined as the distance from the big end to the centre of gravity of the connecting rod.

Similarly to what has been done for the forces, these six moments need to be time shifted with the phase shifting $\{0, 120, 240, 240, 120, 0\}$.

The final moment along the \hat{i} axis will be:

$$\bar{M}_x = \sum \bar{M}_{cri} \quad (28)$$

Regarding the other two moments along \hat{j} and \hat{k} , the equations will be:

$$M_y = \sum_{i=1}^6 (O_{cyl_i} - O) \times F_{z_i} \hat{k} \quad (29)$$

$$M_z = \sum_{i=1}^n (O_{cyl_i} - O) \times F_{y_i} \hat{j} \quad (30)$$

Where $(O_{cyl_i} - O)$ represents the distance between the centre of mass of the i^{th} piston and the centre of mass of the engine.

Every part of the Lagrangian equation **(1)** has been now defined.

2.2.4. Final Lagrangian equations

By substituting all the terms into equation **(1)**, the following system is obtained:

$$\left\{ \begin{array}{l} m\ddot{x}_G + 4kx_G - 4kd_{xz}\theta_y = 0 \\ m\ddot{y}_G + 4ky_G - 4kd_{yz}\theta_x = F_y \\ m\ddot{z}_G + 4kz_G = F_z \\ I_{11}\ddot{\theta}_x + I_{12}\ddot{\theta}_y + I_{13}\ddot{\theta}_z + 4kd_{yz}y + 8k d_{yz}^2\theta_x = M_x \\ I_{21}\ddot{\theta}_x + I_{22}\ddot{\theta}_y + I_{23}\ddot{\theta}_z - 4kd_{xz}x + 8k d_{xz}^2\theta_y = 0 \\ I_{31}\ddot{\theta}_x + I_{32}\ddot{\theta}_y + I_{33}\ddot{\theta}_z + 8k d_{xy}^2\theta_z = 0 \end{array} \right. \quad (31)$$

This final system represents all the six equations of motion of the problem can also be written in matrix form:

$$[m]\ddot{\bar{x}} + [K]\bar{x} = \bar{F} \quad (32)$$

Where $\ddot{\bar{x}}$ is the acceleration vector, \bar{x} is the displacement vector, \bar{F} is the forcing vector, $[M]$ is the mass matrix and $[K]$ is the stiffness matrix.

The contribution to the motion given by the dampers can be written as $[C]\dot{x}$, where $[C]$ is the damping matrix. Damping matrix has been calculated with the proportional approach, which means that it can be seen as a linear combination of the mass and the stiffness matrices:

$$[C] = \alpha[M] + \beta[K] \quad (33)$$

Thanks to the geometry of the problem, the damping matrix will have the same shape of the stiffness matrix, with c instead of k , meaning that $\alpha = 0$, and $\beta = \frac{c}{k}$.

The final equation of government of the system will therefore be:

$$[m]\ddot{\bar{x}} + [C]\dot{\bar{x}} + [K]\bar{x} = \bar{F} \quad (34)$$

Where the obtained matrices are as follows:

$$[M] = \begin{bmatrix} m & 0 & 0 & 0 & 0 & 0 \\ 0 & m & 0 & 0 & 0 & 0 \\ 0 & 0 & m & 0 & 0 & 0 \\ 0 & 0 & 0 & J_{xx} & J_{xy} & J_{xz} \\ 0 & 0 & 0 & J_{yx} & J_{yy} & J_{yz} \\ 0 & 0 & 0 & J_{zx} & J_{zy} & J_{zz} \end{bmatrix} \quad (35)$$

$$[C] = \begin{bmatrix} 4c & 0 & 0 & 0 & -4cd_{xz} & 0 \\ 0 & 4c & 0 & 4cd_{yz} & 0 & 0 \\ 0 & 0 & 4c & 0 & 0 & 0 \\ 0 & 4cd_{yz} & 0 & 8cd_{yz}^2 & 0 & 0 \\ -4cd_{xz} & 0 & 0 & 0 & 8cd_{xz}^2 & 0 \\ 0 & 0 & 0 & 0 & 0 & 8cd_{xy}^2 \end{bmatrix} \quad (36)$$

$$[K] = \begin{bmatrix} 4k & 0 & 0 & 0 & -4kd_{xz} & 0 \\ 0 & 4k & 0 & 4kd_{yz} & 0 & 0 \\ 0 & 0 & 4k & 0 & 0 & 0 \\ 0 & 4kd_{yz} & 0 & 8kd_{yz}^2 & 0 & 0 \\ -4kd_{xz} & 0 & 0 & 0 & 8kd_{xz}^2 & 0 \\ 0 & 0 & 0 & 0 & 0 & 8kd_{xy}^2 \end{bmatrix} \quad (37)$$

2.3. Modal analysis

With the matrices found in chapter **2.2.4**, it's possible to continue with the modal analysis in order to find the mode shapes and the natural frequencies of the system.

For this purpose, the first step is solving the frequency equation:

$$\det([K] - \omega[m]) = 0 \quad (38)$$

This equation yields the natural frequencies of the system ω_i .

By substituting each natural frequency in the frequency equation, it is possible to find the mode shapes:

$$([K] - \omega_i[m]) \vec{X}_i = 0 \rightarrow \vec{X}_i = \begin{Bmatrix} X_i^1 \\ X_i^2 \\ X_i^3 \\ X_i^4 \\ X_i^5 \\ X_i^6 \end{Bmatrix} \quad (39)$$

The modal matrix $[X]$ is now defined as:

$$[X] = [\vec{X}_1 \vec{X}_2 \vec{X}_3 \vec{X}_4 \vec{X}_5 \vec{X}_6] \quad (40)$$

The values of the modal matrix are then chosen in order to normalize the inertia matrix:

$$[X]^T[m][X] = [I] \quad (41)$$

With this normalized modal matrix is now possible to calculate the modal stiffness matrix:

$$[X]^T[K][X] = [\nwarrow \omega^2 \searrow] = \begin{bmatrix} \omega_1^2 & \cdots & 0 \\ \vdots & \ddots & \vdots \\ 0 & \cdots & \omega_6^2 \end{bmatrix} \quad (42)$$

2.4. Time response

The relationship between generalized coordinates and modal coordinates is defined as:

$$\bar{x}(t) = [X]\bar{q}(t) \quad (43)$$

Substituting equations (33) and (43) in the equation (34), the result is:

$$[M][X]\ddot{\bar{q}} + [\alpha[M] + \beta[K]][X]\dot{\bar{q}} + [K][X]\bar{q} = \bar{F} \quad (44)$$

By pre-multiplying by $[X]^T$ it can be obtained that:

$$[I]\ddot{\bar{q}} + [\alpha[I] + \beta[\nabla \omega^2 \Delta]]\dot{\bar{q}} + [\nabla \omega^2 \Delta]\bar{q} = [X]^T \bar{F} = \bar{Q} \quad (45)$$

For the i component we have:

$$\ddot{q}_i + (\alpha + \beta \omega_i^2)\dot{q}_i + \omega_i^2 q_i = Q_i \quad (46)$$

The term $(\alpha + \beta \omega_i^2)$ can also be written as $2\zeta_i \omega_i^2$. For the case in exam, it is easy to see that, since α is 0, the value of ζ_i can be easily found with the following relation:

$$\zeta_i = \frac{\beta \omega_i}{2} \quad (47)$$

To obtain the time response in terms of generalized coordinates $\bar{x}(t)$, first it is necessary to calculate the time response in modal coordinates $\bar{q}(t)$, which means applying the convolution integral to each of the six equations of motion in modal form: these equations are uncoupled, so the solution is simply a system of six single degree of freedom problems.

The modal coordinates are calculated as follows:

$$q_i(t) = \frac{1}{\omega_{di}} \int_0^t Q_i(\tau) e^{-\zeta_i \omega_i (t-\tau)} \sin(\omega_{di}(t-\tau)) d\tau \quad (48)$$

Where only the component related to the forces has been considered. The response due to the initial conditions has been considered zero.

For clarity, it's useful to remember that:

$$\omega_{di} = \omega_i \sqrt{1 - \zeta_i^2} \quad (49)$$

The time response in the generalized coordinates $\bar{x}(t)$, is given by:

$$\bar{x}(t) = [X]\bar{q}(t) \quad (50)$$

2.5. Forces transmitted to the chassis

In order to calculate the forces transmitted to the chassis, a simple rigid body diagram may be used.

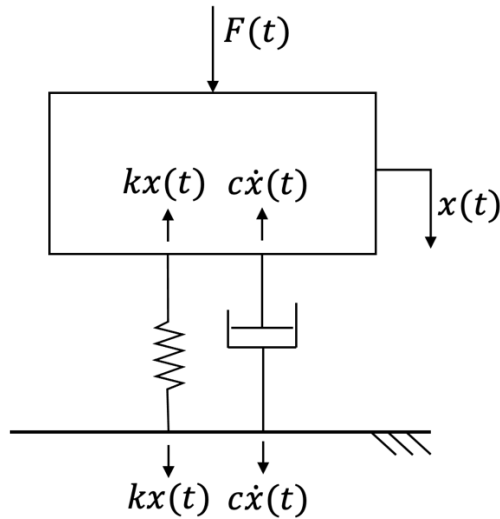


Figure 4 – Forces transmitted to the chassis

As shown in Figure 4, the forces transmitted to the frame are, by Newton's third law, the ones that are generated by the springs and the dampers, with an opposite sign.

So, once the time response has been calculated, as shown in the previous chapter, they can be easily determined by the following equation:

$$\bar{F}_{transmitted}(t) = -([C]\dot{\bar{x}}(t) + [K]\bar{x}(t)) \quad (51)$$

2.6. Spectral analysis

The spectrum of a given function (or signal) is its representation in the frequency domain. Until now, all the development has been carried out in the time domain.

The tool that connects these two domains is the Fourier Transform \mathcal{F} , which is defined as follows:

$$X(\omega) = \int_{-\infty}^{+\infty} x(t)e^{-j\omega t} dt \quad (52)$$

$$x(t) \xrightarrow{\mathcal{F}} X(\omega) \quad (53)$$

The spectrum, as defined in the equation (53), still doesn't have a physical meaning: in order to obtain the real spectrum some operations need to be performed. Firstly, only the spectrum values associated to positive frequencies need to be considered, and secondarily, they have to be multiplied by 2.

Once the spectrum is obtained, it is possible to find out all the frequencies that compose the signal.

3. Numerical implementation

Numerical implementation has been carried out in MATLAB, taking advantage of the existing functions and toolkits to create a parametric simulator, enabling the user to build and test an unlimited amount of inline engines. To do so, a system of interacting classes has been built, following the principles of Object-Oriented Programming (OOP) to encapsulate information and provide a modular and reusable set of tools for researching engine vibrations. Finally, a graphical user interface (GUI) has been connected to the classes, completing the P.I.E. (Parametric Inline Engine) Simulator.

3.1. P.I.E. classes and interactions

The simulator has been designed so that every class corresponds to a real component of the engine.

Piston, crank and conrod classes are characterized by their mass and dimensions, while the cylinder class contains them and is able to calculate the forces that are produced by the crank and slider mechanism, following the method explained in chapter **2.2.3**.

The engine mounts class contain the information relative to stiffness and damping matrices. Both are calculated based on the matrices of chapter **2.2.4**, and k and c have been set to the values shown in chapter **3.2**. The engine dimensions (and therefore the spacing of the mounts) are calculated parametrically, based on the number of cylinders of the engine.

The engine block class role is to store data about mass and inertia tensor, both calculated using the empirical formulae shown in chapter **3.2**.

The engine class is characterized by its cylinders, block and mounts. Its function is to calculate the total forces and moments produced by the cylinders, using an iterative approach.

The engine factory class is a useful interface to the engine class, able to build an engine cylinder by cylinder, assigning to the crankshaft its correct angles and adding defects to the pistons when required. The piston error is used in order to produce more realistic results: based on the dimensional tolerances of the real parts, the user can input a maximum percentage error to the mass of the component, resulting in additional forces and moments that will cause imbalance in the engine. Each piston's mass varies randomly in the interval defined by

$$[m_{ideal}(1 + \%_{max\ error}), m_{ideal}(1 - \%_{max\ error})]$$

Finally, the dyno (abbreviation of dynamic bench) class is used to test the engine and measure the output signals. It can retrieve data from the engine about the forcing inputs, calculate all of the system's characteristics (natural frequencies, mode shapes, et cetera), set the testing revolution speeds and the testing times, measure the time and frequency response and the transmitted forces. In particular, to calculate the system's characteristics the MATLAB function *eig* is used, obtaining the modal matrix and the natural frequencies as the output. For the time

response, the function *conv* is used to perform the convolution integral between the forcing input and the impulse response of the system, while for the frequency response the *fft* function has been exploited. For transmitted forces, the time response vectors have been derived by using the *gradient* function. The whole procedure followed to calculate the response is identical to the one described in chapters **2.3, 2.4, 2.5, 2.6**. The time resolution used by the dyno in all its calculations is set to 10^{-4} s.

A full UML (Unified Modelling Language) class diagram is provided in Figure 5 in order to document how the simulator works.

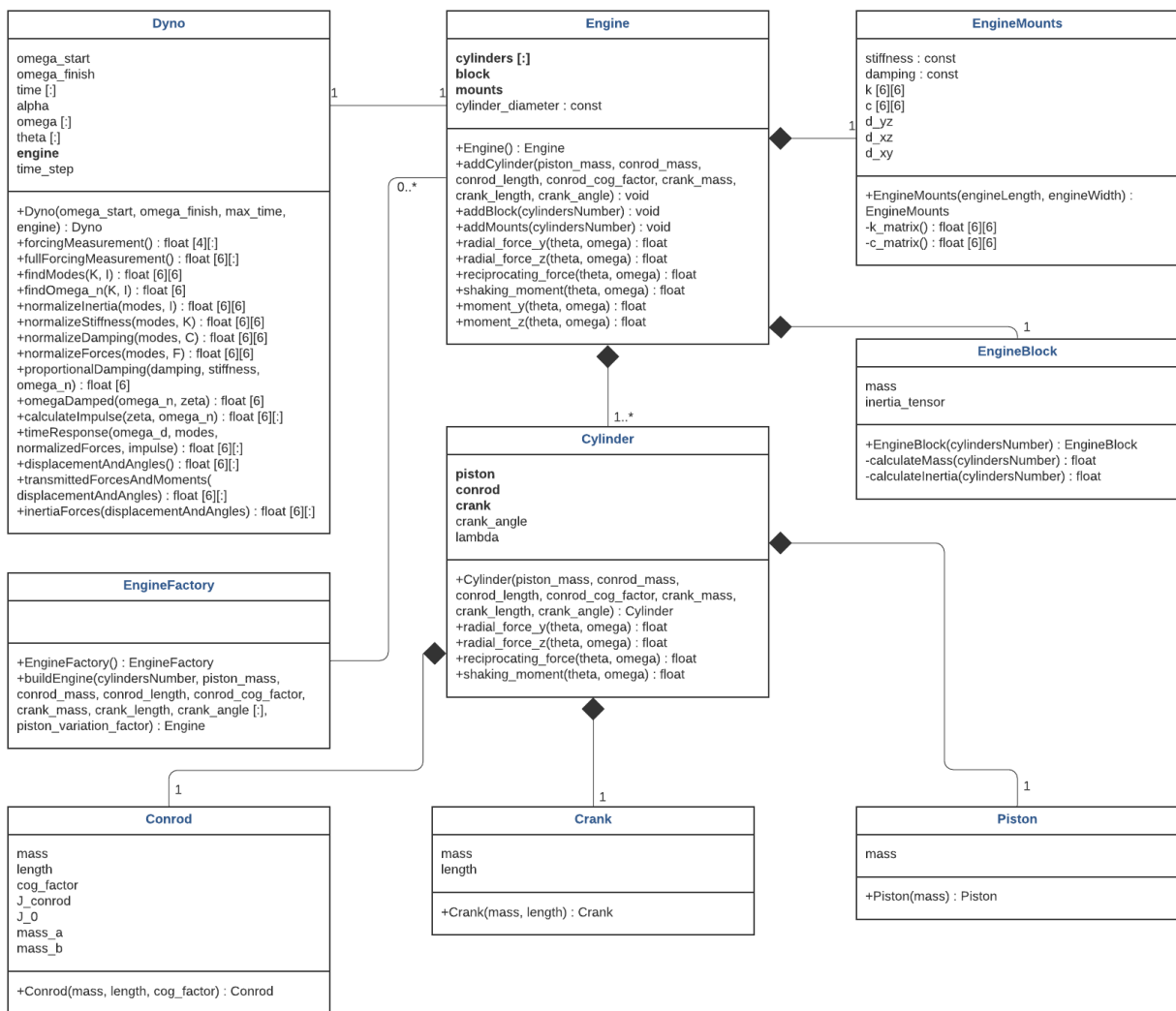


Figure 5 - P.I.E. Simulator UML class diagram

The GUI shown in Figure 6 has been developed in order to let the user input the engine data with ease, even though the classes already provide a simple enough command-line interface. All the geometrical parameters, along with the mass data, testing specifications and defects

level can be set via slider handles, and the simulation is started by a button. A set of other buttons lets the user inspect detailed data for both forcing and response, in addition to the quick overview that the main window provides in the form of four graphs.

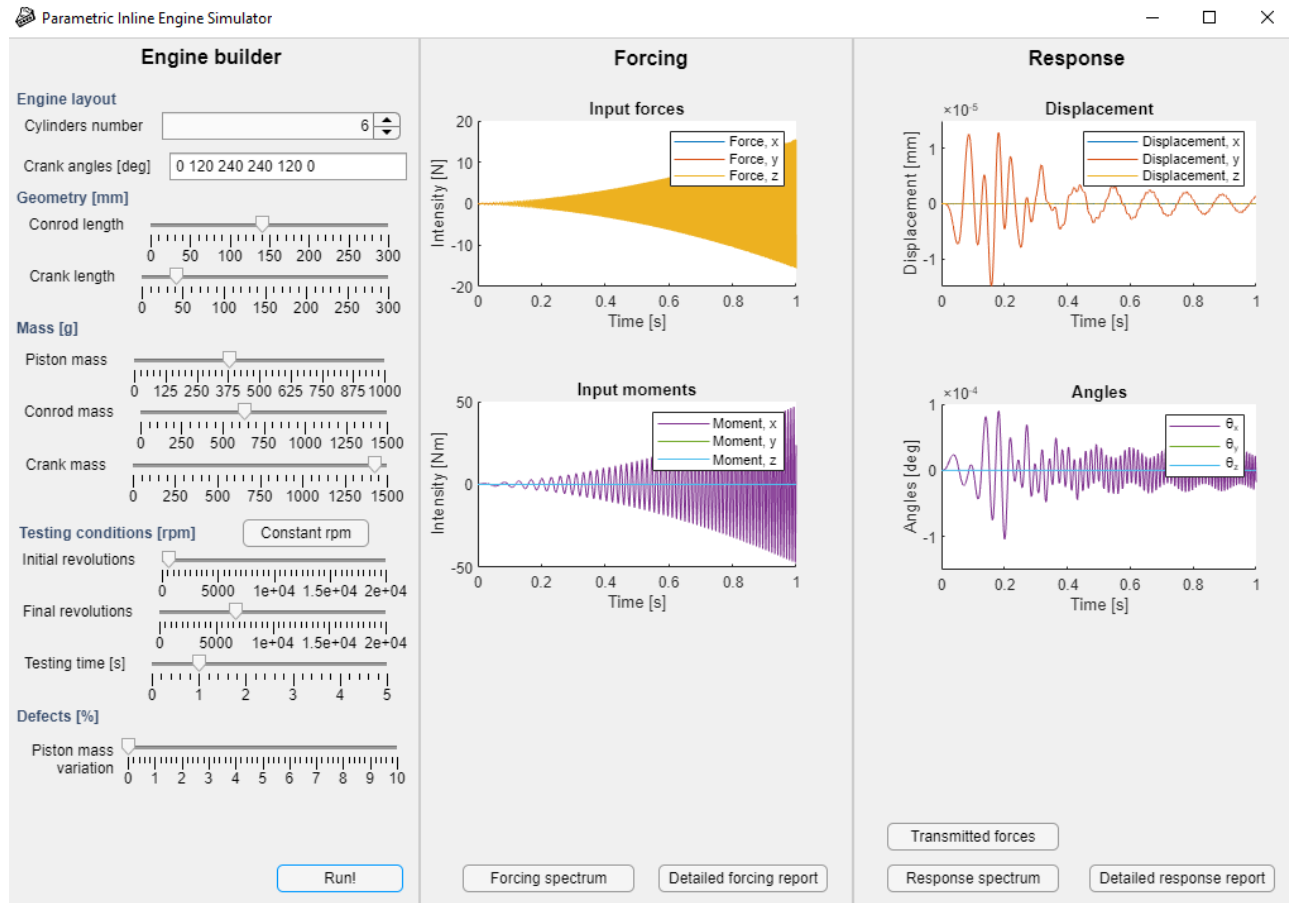


Figure 6 - P.I.E. GUI

3.2. Definition of the engine data

The engine chosen as case study is the Toyota 2-JZ inline-six. Internal parts data and performance curves are widely available on the internet (Table 1).

<i>Spec</i>	<i>Value</i>
Piston mass	380g
Crank mass	1430g
Conrod mass	635g
Crank length	43mm
Conrod length	142mm
Idle	650rpm
Limiter	6800rpm
Max power @	5600rpm
Max torque @	3600rpm

Table 1 - Engine specs and performance data

To recreate an accurate model of the cylinder block, finding reliable data proved to be difficult due to inconsistencies between sources, therefore most of the measurements have been derived from images or existing 3D models. The collected data has then been used to recreate the engine with Autodesk Inventor (Figure 7).



Figure 7 - 6-cylinder block CAD model

The model is composed by three parts: engine block, crankcase and oil sump (Figure 8). The parts were then assembled, obtaining the final data of the engine.

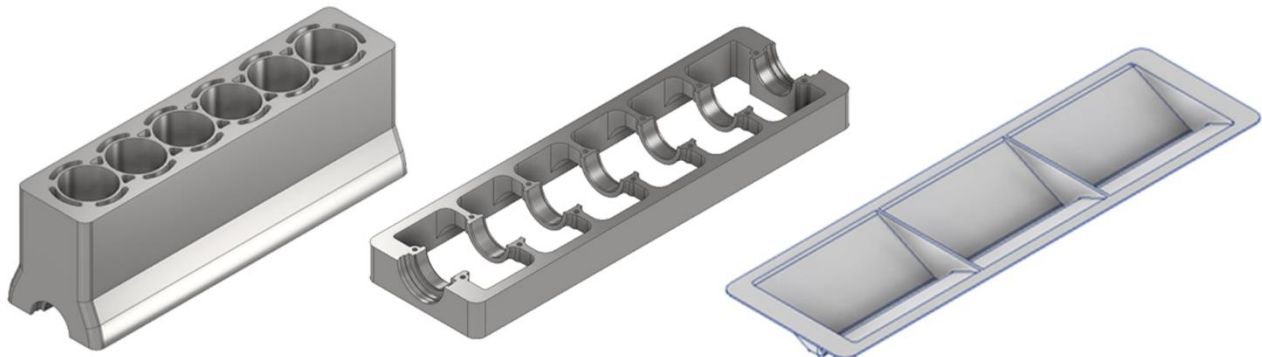


Figure 8 - Engine parts

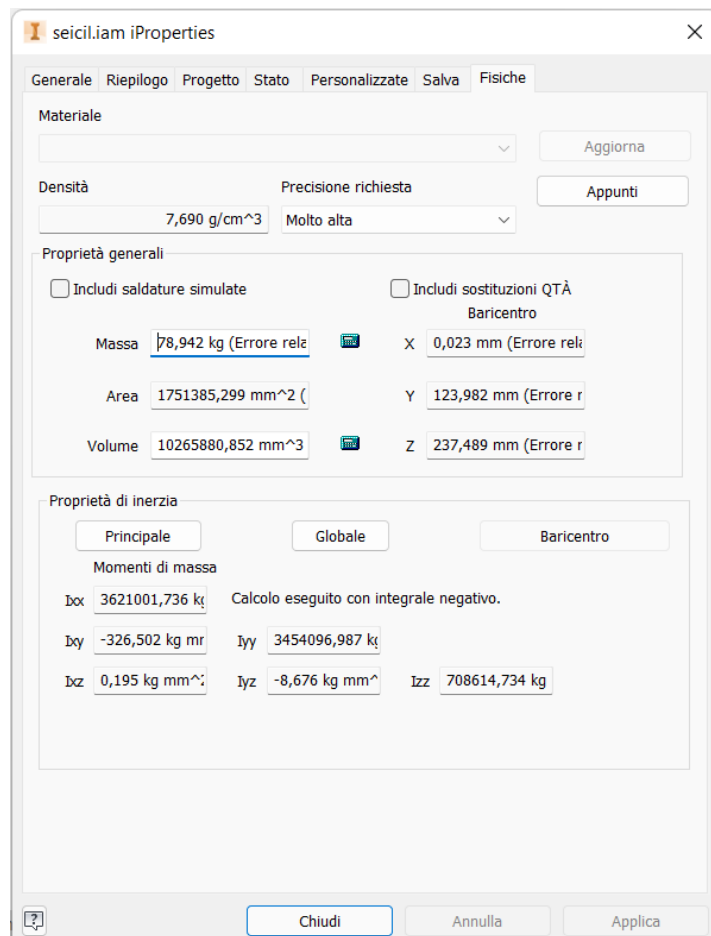


Figure 9 - Mass and inertia tensor calculated by the CAD software

Furthermore, in order to allow the creation of a parametric model of the mass ad inertia tensor, three other CAD models were created (single-cylinder block, three-cylinder block, ten-cylinder block). Their inertia tensors were then calculated and further elaborated to create empirical laws defining the characteristics of the engine block based on the number of cylinders, as shown in Table 2.

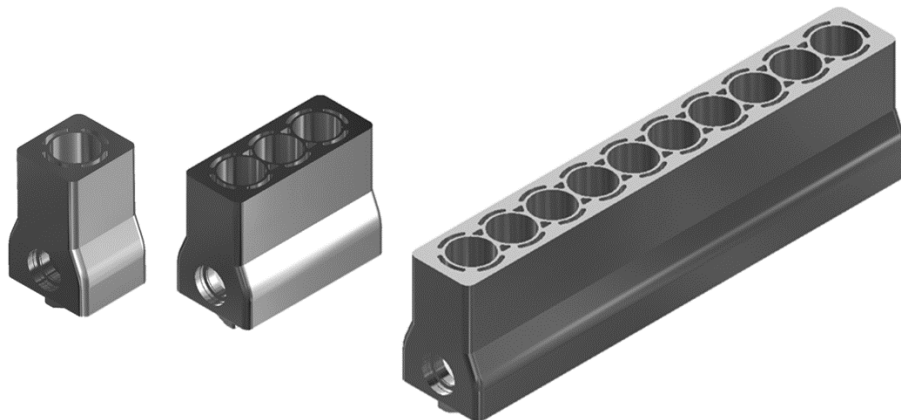


Figure 10 - Additional CAD models used to calculate parametric laws

<i>Engine property</i>	<i>Expression</i>
Mass [kg]	$12.659 n$
J_{xx} [kg m²]	$\frac{8712.2 n^3 + 20270 n^2 + 177514 n - 55634}{10^6}$
J_{yy} [kg m²]	$\frac{5715.8 n^3 + 72699 n^2 + 75560 n}{10^6}$
J_{zz} [kg m²]	$\frac{121238 n}{10^6}$
J_{xy} [kg m²]	$\frac{-157.5 \log(n) + 152.12}{10^6}$
J_{xz} [kg m²]	$\frac{-21.67 \log(n) + 58.436}{10^6}$
J_{yz} [kg m²]	$\frac{-6.364 \log(n) - 5.3237}{10^6}$

Table 2 - Engine properties empirical laws

Finally, since the parametric model allows the study of the behaviour of the engine under randomized mass variations of the piston, it has been necessary to define the upper and lower percentage weight limits.

Taking advantage of the dimensional tolerances of the piston found in literature, it has been possible to model a simplified CAD model of the piston. The values of the mass have been measured using the “Mass properties” tool of the CAD software SolidWorks 2016, defining aluminium as material.

The three weight conditions that have been considered are: minimum dimension, maximum dimension, nominal dimension. While the dimensions that have been affected by the tolerances are external diameter, internal diameter, height and head thickness. The results of the measurements and the tolerances are listed in the following table.

Condition	Weight [g]	External Diameter [mm]	Internal diameter [mm]	Height [mm]	Head thickness [mm]
Nominal	300.95	86	78	68	8
Minimum	287.9	85.917	78.3	67.7	7.7
Maximum	310.06	85.927	77.7	68.3	8.3

Table 3 - Piston weights and dimensions

Lastly, the percentage weight variations were evaluated as follows:

$$\%WV_{MAX} = \frac{\text{Maximum weight} - \text{Nominal weight}}{\text{Nominal weight}} * 100$$

$$\%WV_{min} = \frac{\text{Minimum weight} - \text{Nominal weight}}{\text{Nominal weight}} * 100$$

The results are:

$$\%WV_{MAX} = 3.2\%$$

$$\%WV_{min} = -4.3\%$$

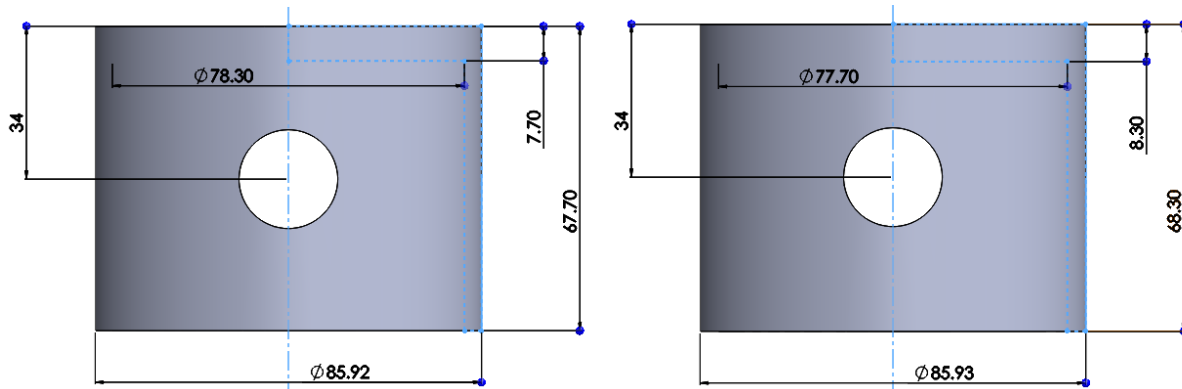


Figure 11 - Piston dimensions in the minimum and maximum weight conditions

The values of stiffness and damping of the real engine mounts are frequency-dependant: experimental data of stiffness and damping ratio is available [2], but for the sake of simplicity, an arithmetical average is considered in various frequency ranges. From the average values of damping ratio, the damping value is obtained in reverse with respect to the usual procedure (using the relative data).

<i>Stiffness [N/mm]</i>	<i>Damping ratio</i>
100	0.16
90	0.23
120	0.19
140	0.13
160	0.09
150	0.04
150	0.024
170	0.02
160	0.013
180	0.015
200	0.005
130	0.005
150	0.008
300	0.01
150	0.013

Table 4 - Stiffness and damping ratio data

$$k = 156666.7 \frac{N}{m} \quad c = 158.4 \frac{N}{ms}$$

4. Simulation results

4.1. Static measurements: determination of system parameters

As a first simulation step, the dynamic bench has been set up to keep the engine shut down and measure the parameters of the system. Calculating the modal shapes and the natural frequencies already showed interesting results: the first two natural frequencies are, in fact, found under the idle regime of the engine. It is clear, then, that these two frequencies will never be met under normal driving conditions, and that the engine would not be able to run for long at that speed even when forced to, making them completely unnoticeable at any steady revolution regime, and only noticeable in the transient response of the engine.

The damping ratios of the system are all well under the critical value, as expected for a mechanical system like the one in exam, where the damping of the mounts is “incidental”.

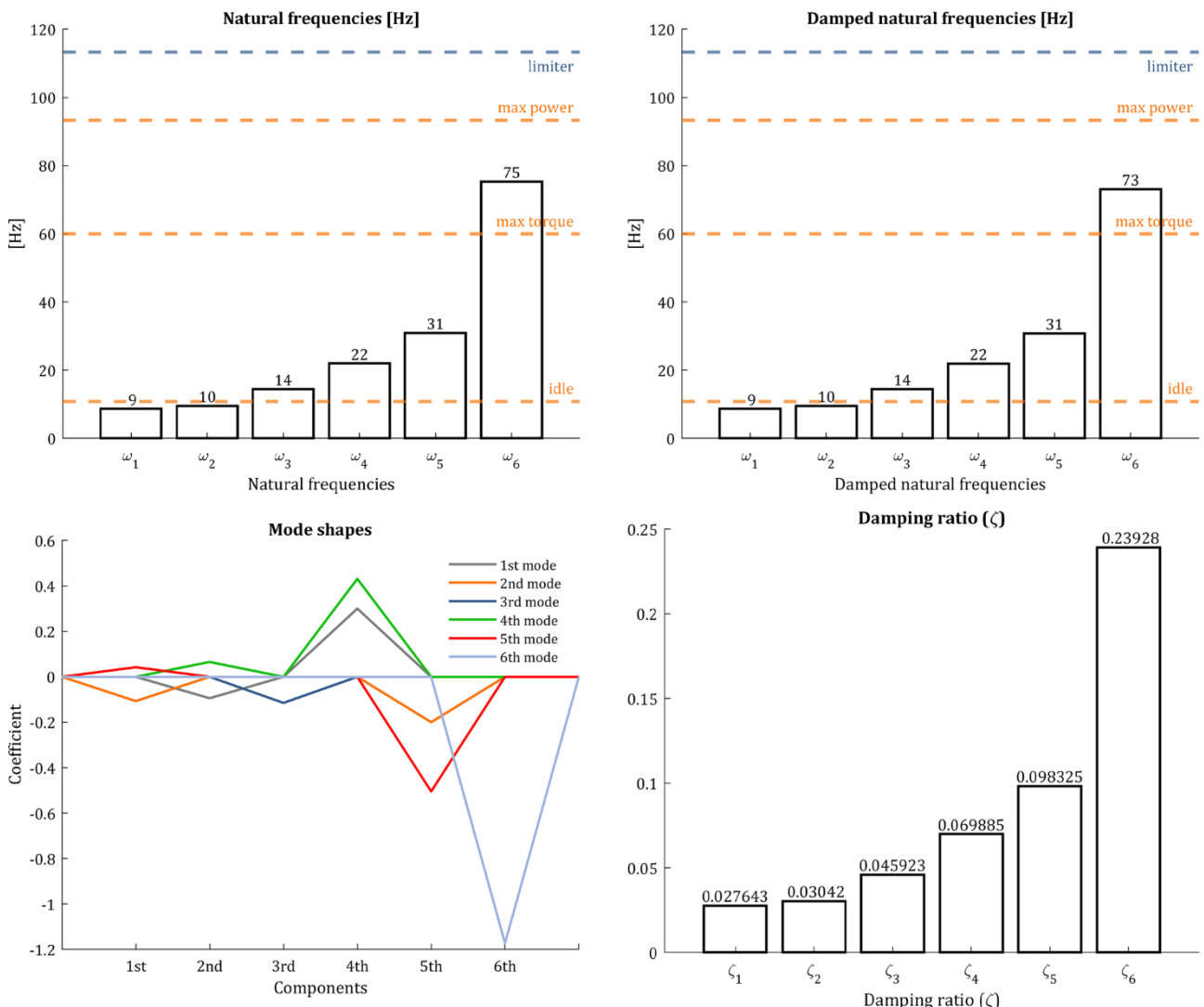


Figure 12 - Static measurements results
Mechanical Vibrations course – 2021/2022

4.2. Speed ramp: from idle to limiter

A speed ramp going from idle to limiter regime has been investigated. The testing time chosen for this test is 5 seconds, in order to let the engine settle reasonably well on the variable forcing frequency.

Forces on the y and x axis are null, the former as a result of the summation of all cylinders at different phase shifts, and the latter due to the simple lack of forces along that axis. Forces along the z axis, instead, remain.

Moments on the z and y directions are null, due to the symmetric shape of the crankshaft (compared to the center of the engine). Moments on the x axis are instead caused by the connecting rod movement and do not cancel each other out.

Both forces and moments scale with the square of the revolution speed, causing the parabolic shape clearly noticeable in Figure 13.

It's clear that the springs' displacements are reduced at higher excitation speeds, showing that the system has a lower transmissibility in that range, while the first oscillations show larger amplitudes thanks to the transient response characteristics of an underdamped system.

In the spectral analysis (Figure 14), it is possible to observe the typical *sweep* shape of the excitation, showing only one profile for the forces and two for the moments, showing a different number of orders for the two forcing inputs.

Displacements, angles and transmitted forces and moments show that the engine indeed works as a lowpass filter, showing a rapid decrease in amplitude at higher frequencies compared to the lower ones. Additionally, all the spectra show pronounced peaks in correspondence of the natural frequencies, especially noticeable at 9 and 10 Hz, due to the transient response being part of the simulation data.

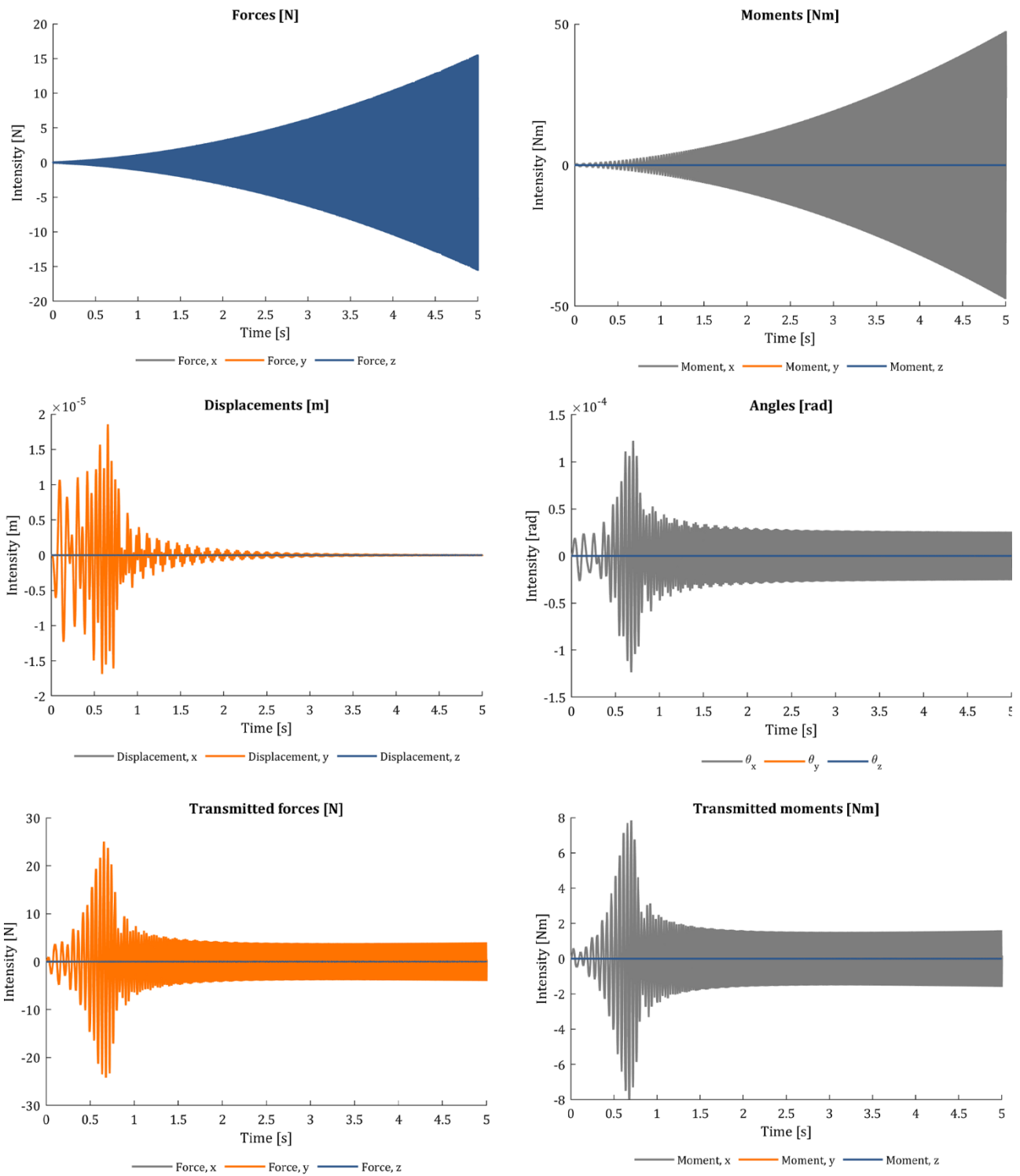


Figure 13 – Speed ramp simulation - time domain signals representation

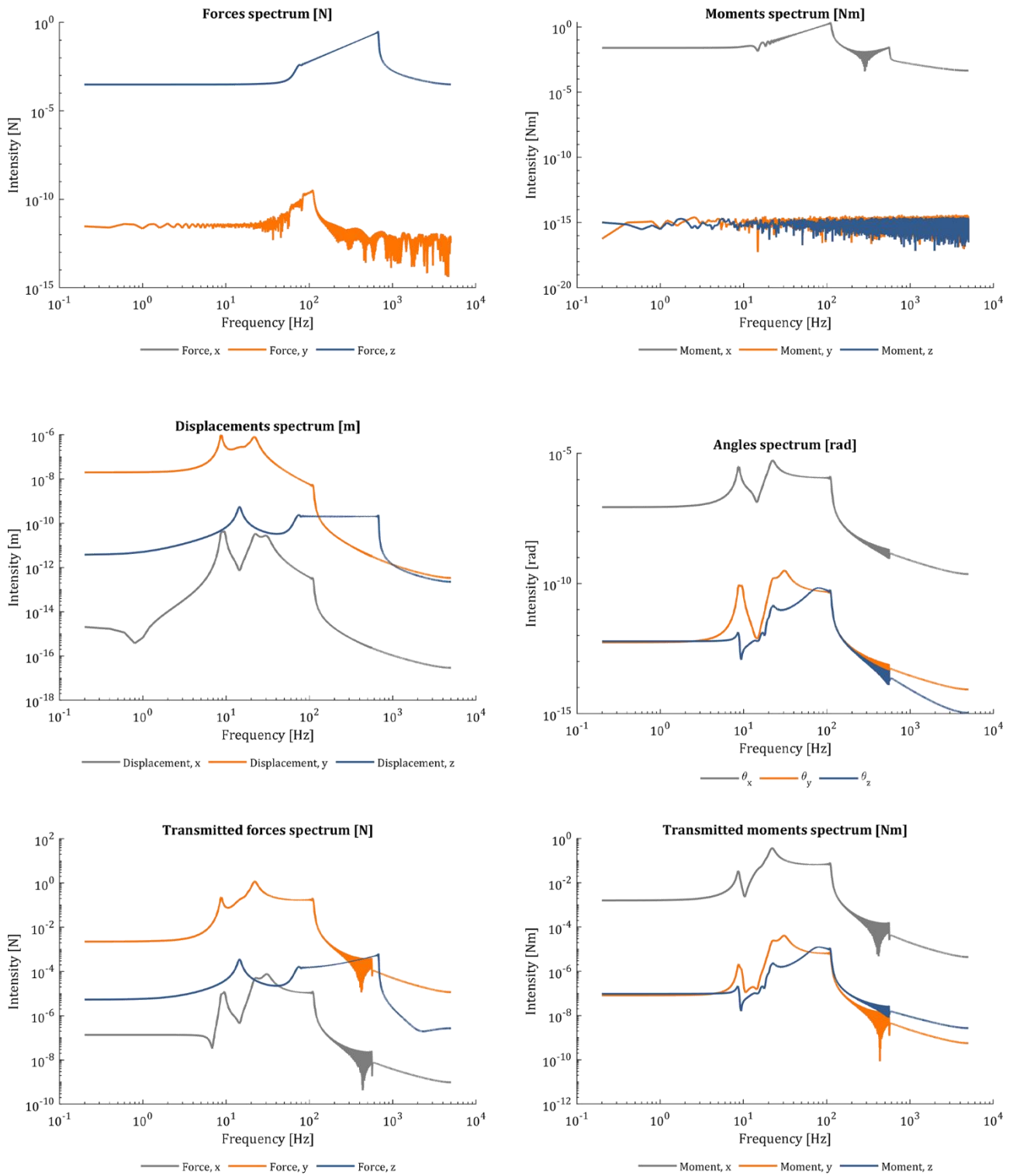


Figure 14 - Speed ramp simulation - frequency domain signals representation

4.3. Steady forcing: idle regime

At idle regime, forcing inputs have very low intensity (Figure 15). This is due to the fact that the inline-six, with this crankshaft configuration, is an extremely balanced engine, which cancels out forcing up to the sixth order for forces (while the moments given by the connecting rods keep the first and fifth order), in addition to cancelling out forces and moments on two out of three axes completely. This is easily verified from the spectra of Figure 16, where a peak is visible in the forces graph at a frequency of 65 Hz, precisely 6 times the crankshaft rotation speed (650 rpm or 10.8 Hz).

As for the speed ramp simulation, the transient response is included, highlighting once more the peaks in the response in correspondence of the natural frequencies.

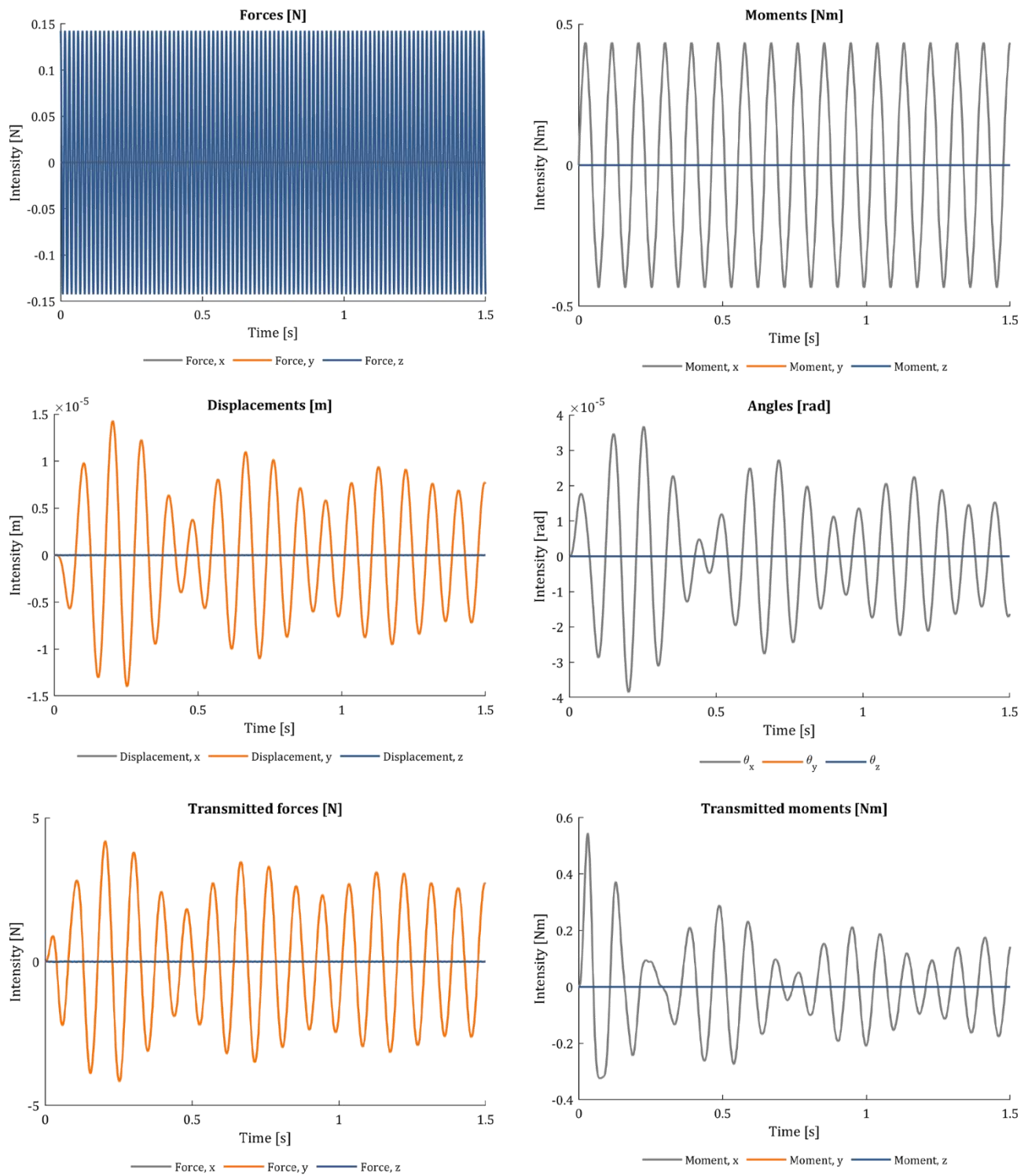


Figure 15 - Idle simulation - time domain signals representation

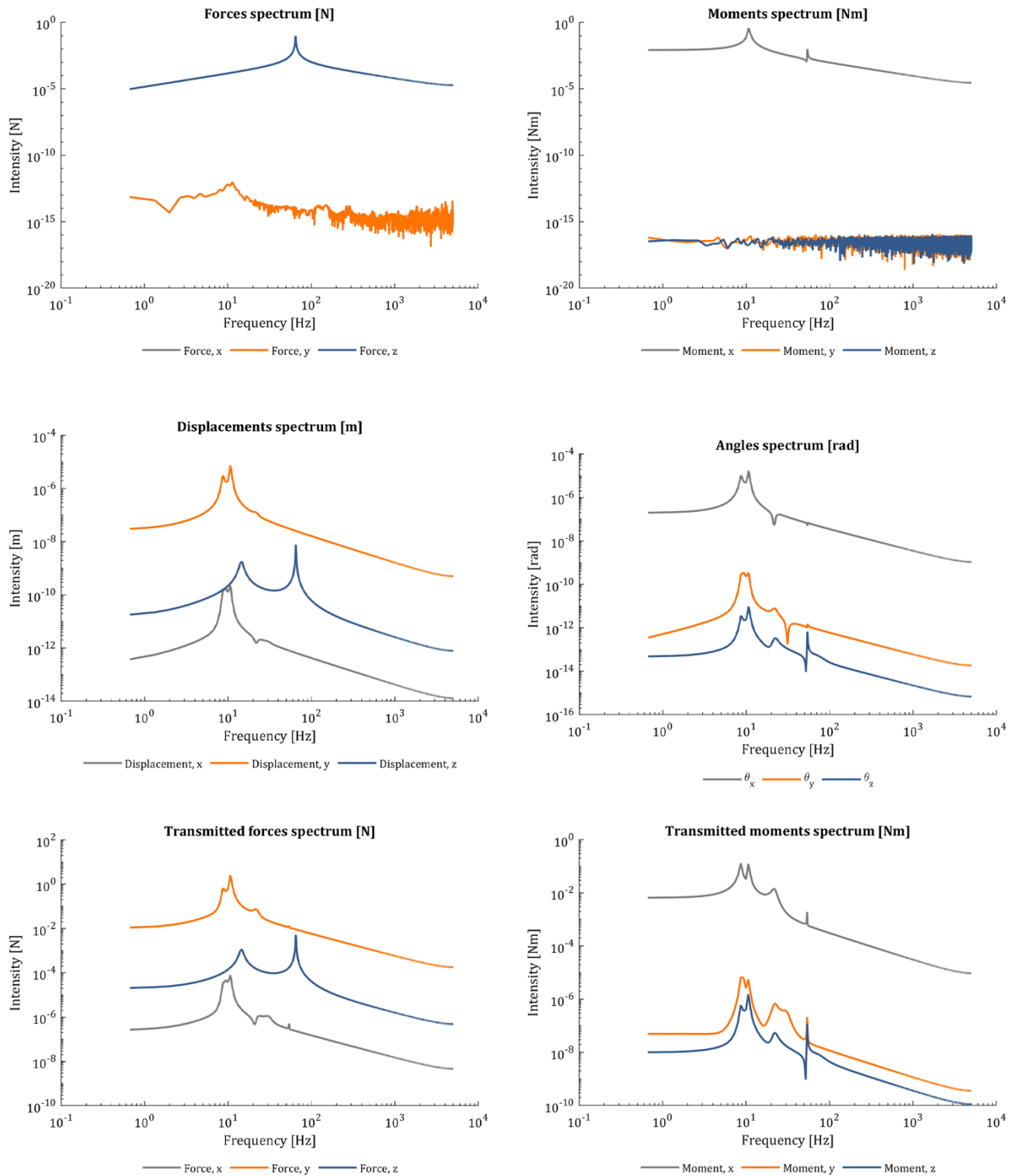


Figure 16 - Idle simulation - frequency domain signals representation

4.4. Steady forcing: maximum power regime

A simulation at the maximum power point of the engine has been performed, in order to investigate the engine's behavior in the speed range that would be typical of a use for racing.

Forcing intensity is still very low, as displacements and angles do.

Again, the spectra highlight peaks in correspondence of natural frequencies, but with a more evident stress on the higher frequencies, due to the faster forcing action.

More interesting results will be brought up for this revolution speed in chapter **4.6**.

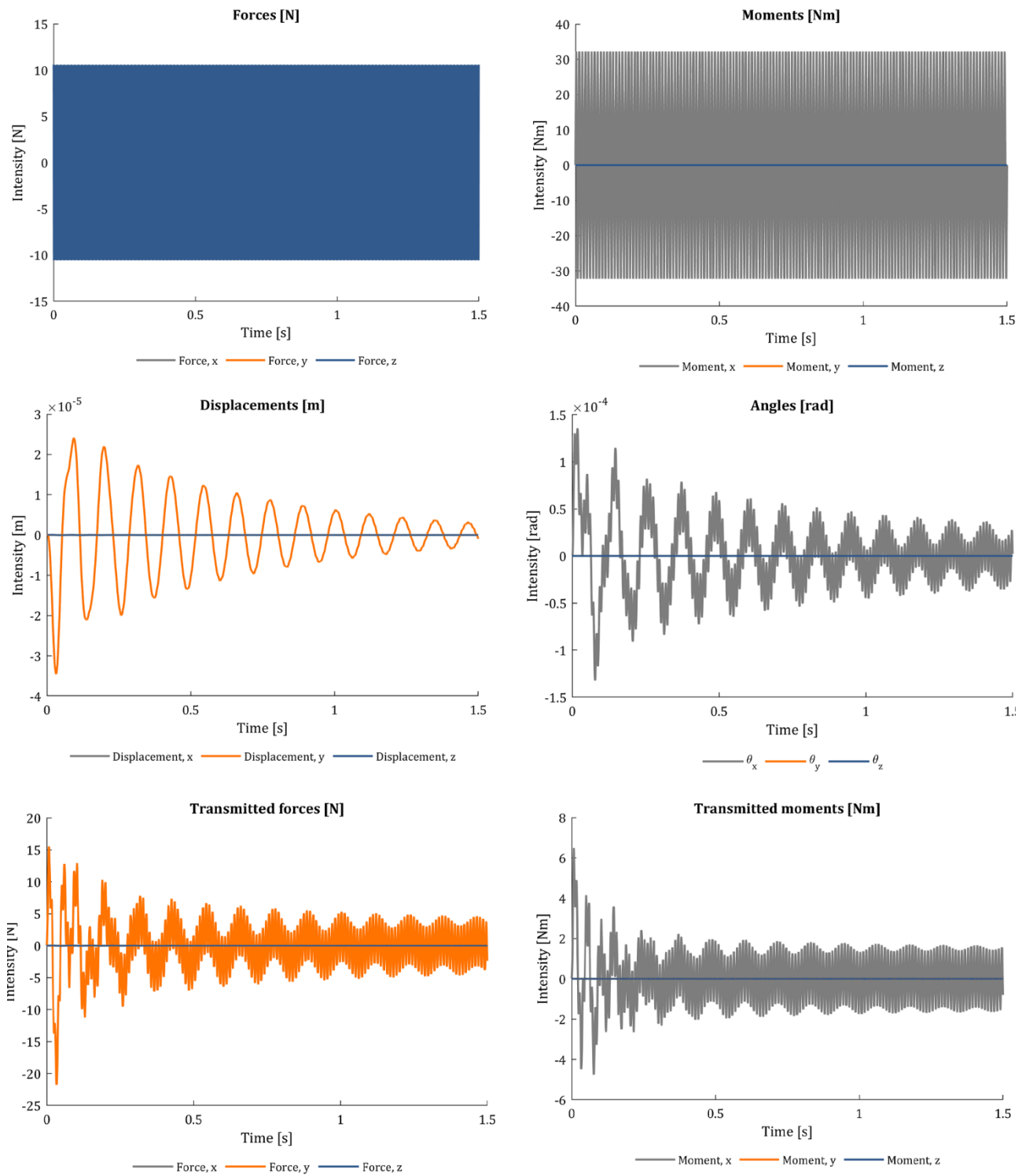


Figure 17 - Maximum power regime simulation - time domain signals representation

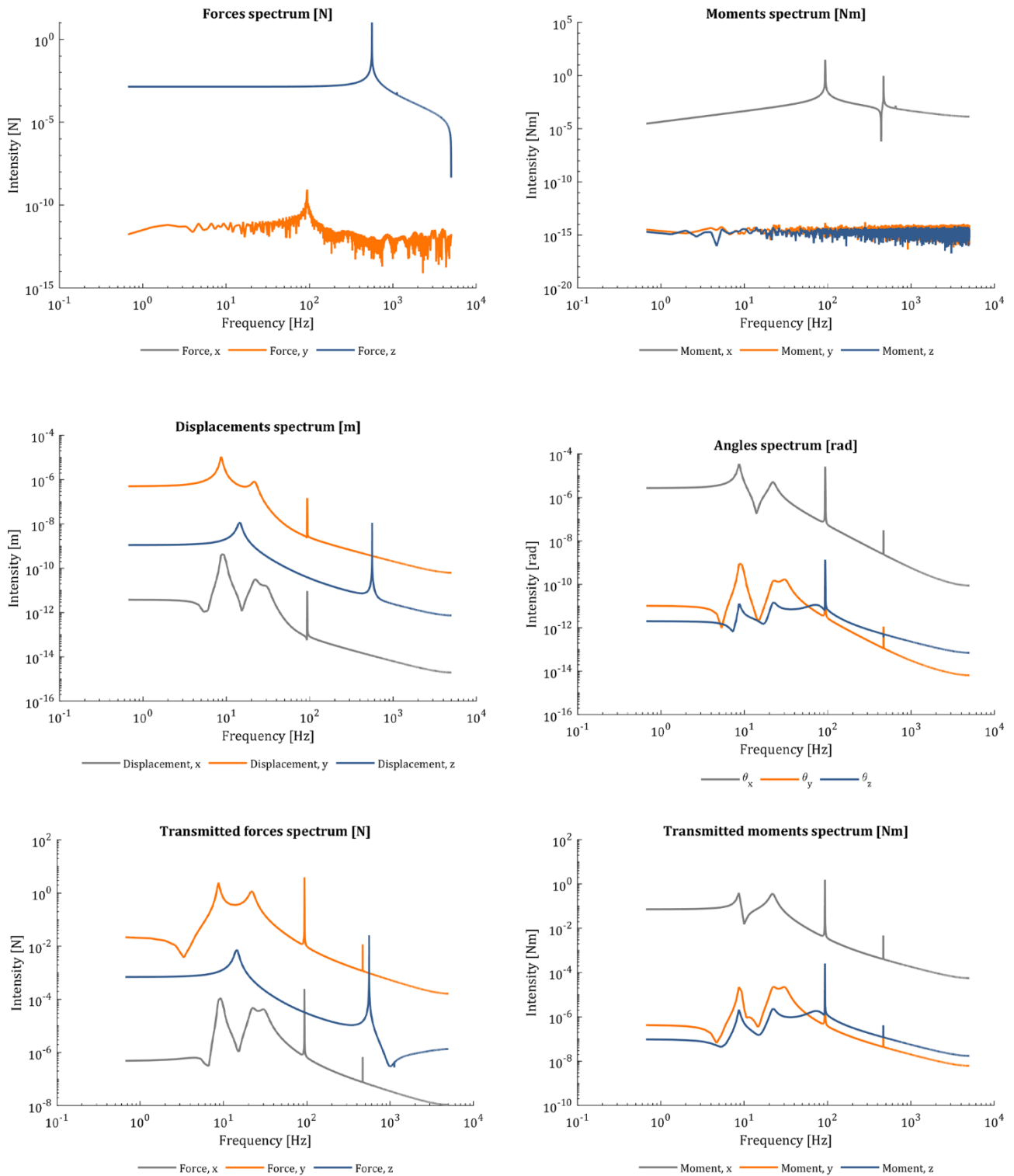


Figure 18 - Maximum power regime simulation - frequency domain signals representation

4.5. Steady forcing: limiter regime

At limiter regime, forces reach their maximum values, and so do the moments.

Even in these conditions, the input forcing is rather limited, but another engine order is shown by the spectrum (Figure 20): the 12th order is now visible, although very limited in amplitude, and therefore of scarce importance for the study of the vibrations of this system.

Displacements and rotations still do not exceed 10^{-5} m and 10^{-4} radians respectively.

In general, anyways, the three steady forcing regime simulations have highlighted the evident smoothness of the engine operation, due to the lack of low-order forcing components and to the first two natural frequencies being well under the normal driving regimes. Such a behavior is shared with other well-balanced engines such as the V12 60° engine, which, similarly to the inline-six, cancels out orders up to the sixth.

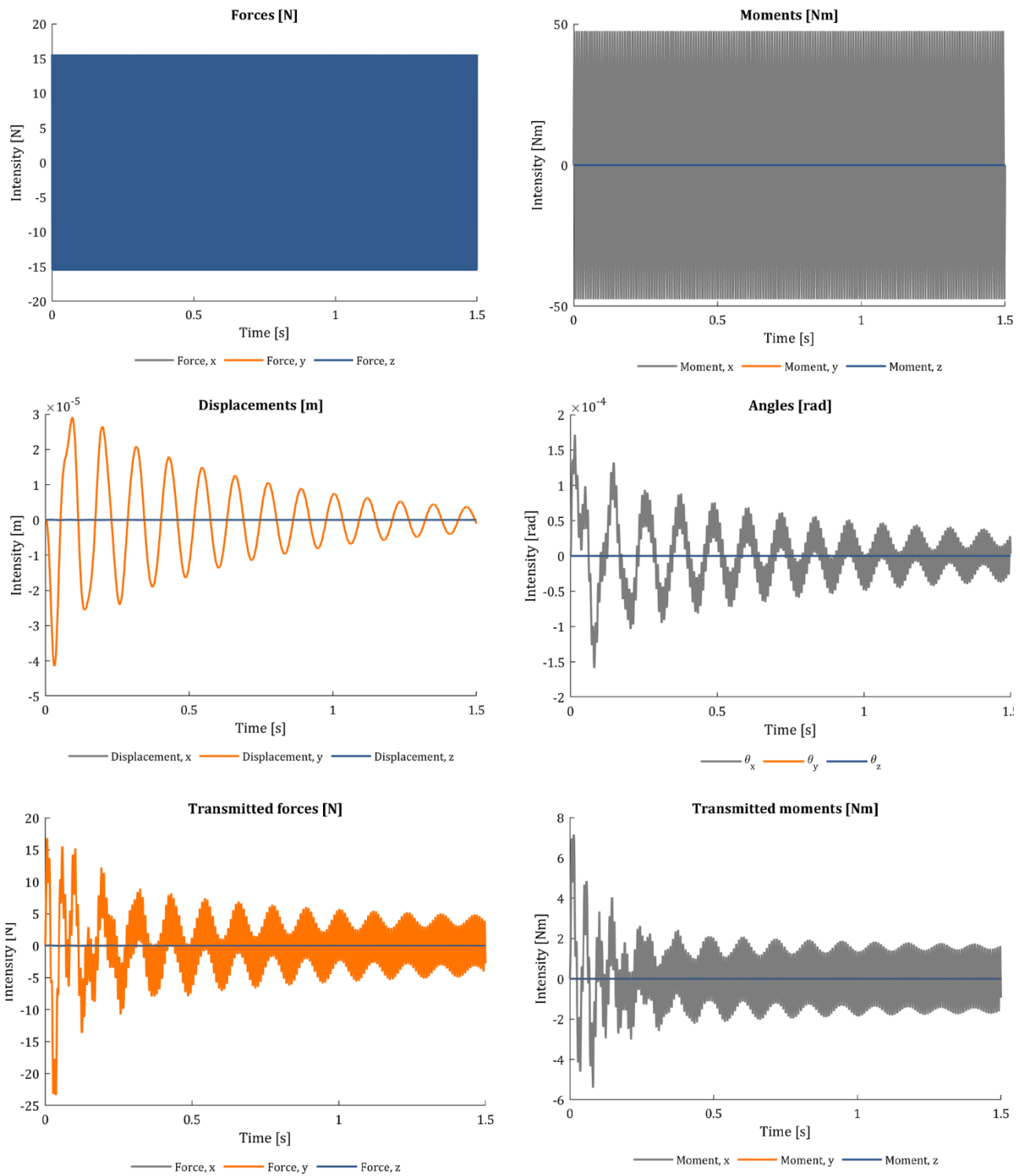


Figure 19 - Limiter simulation - time domain signals representation

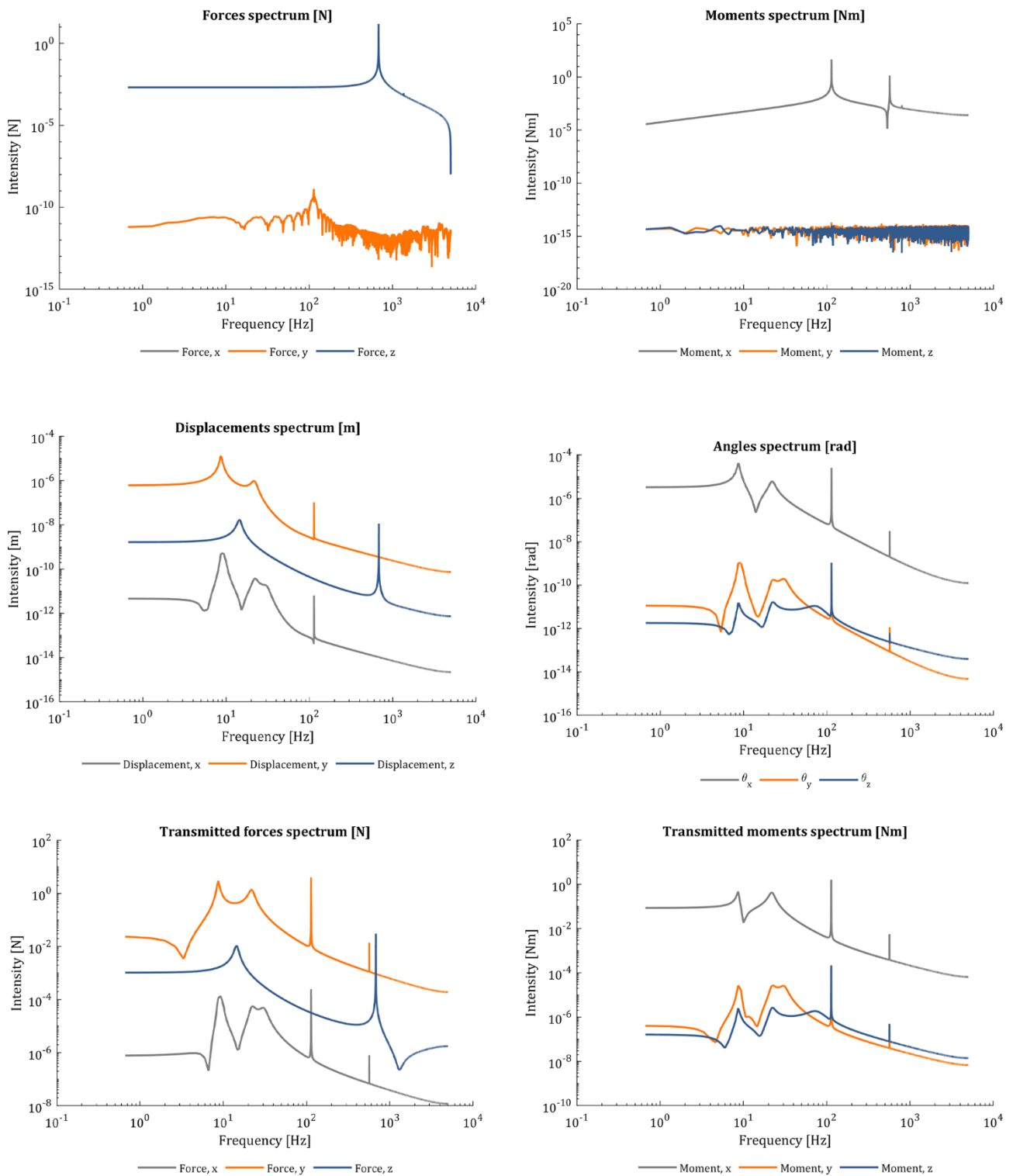


Figure 20 - Limiter simulation - frequency domain signals representation

4.6. Real engine simulation: maximum power regime

Based on the tolerances found in chapter 3.2, another simulation has been run at the maximum power point of the engine.

This time, the ideal engine has been modified by adding or subtracting a randomized mass up to 3.5% of the nominal one to each piston. The result is an inherently imbalanced engine in which forcing orders do not cancel out anymore, causing the forcing to grow by almost two orders of magnitude compared to the ideal case.

This shows how fundamental manufacturing tolerances are in the case of engines such as the inline-six, where forces are naturally low and even small defects lead to rather large increases in forcing inputs. The same cannot be said for engines such as the inline-four, where the second order forcing is naturally present and of much higher intensity than any forcing due to defects in piston masses, therefore allowing for less strict tolerances and a less expensive manufacturing process.

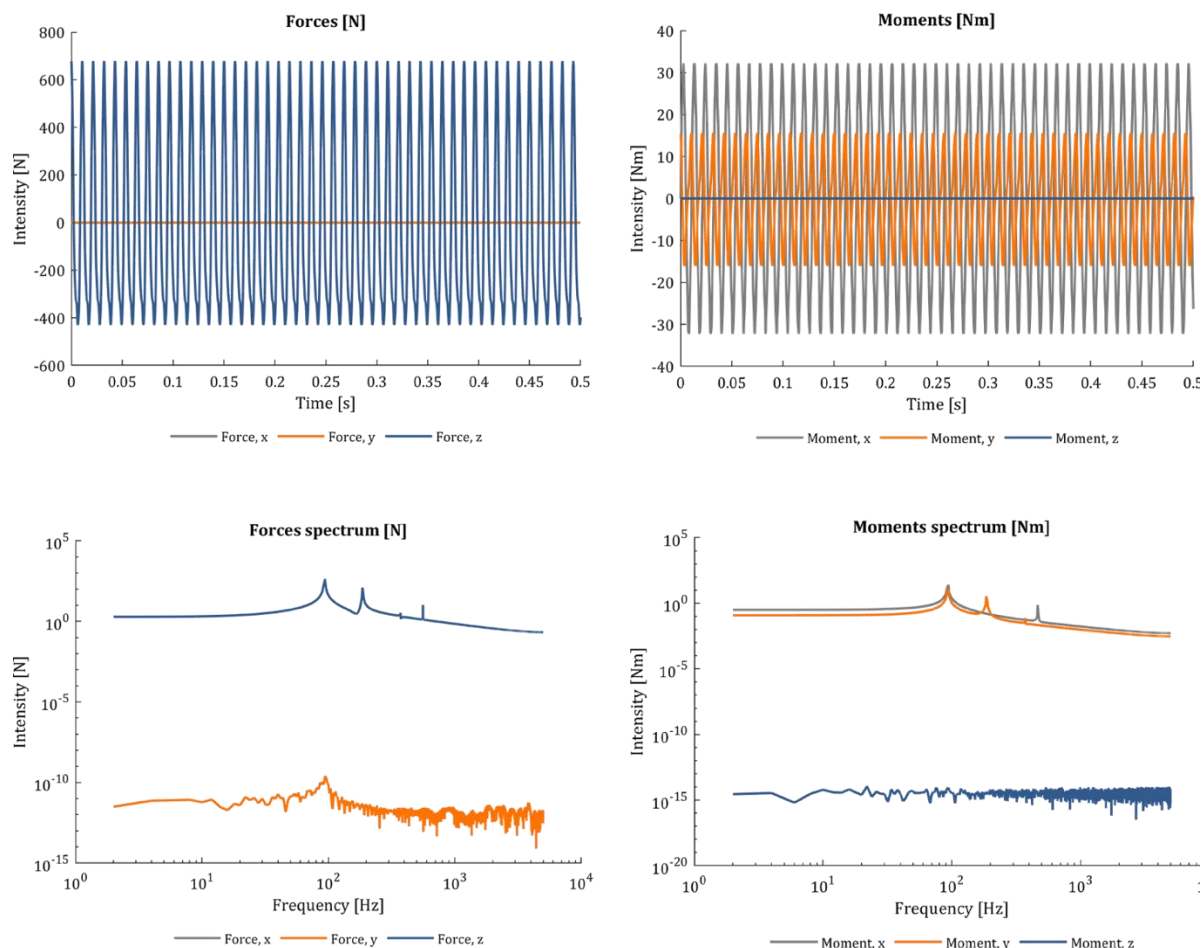


Figure 21 - Real piston mass defects simulation - forcing representation

Mechanical Vibrations course – 2021/2022

4.7. Experimental validation: resonance and error analysis

To further validate the correctness and robustness of the model, two experiments have been carried out, the first of which involves an analysis of the time response to a resonance frequency. The resonance frequency in question is the first one (522.1 rpm), therefore inferior than the idle speed, meaning that the engine will never actually work in this regime. However, the results are still very interesting since they precisely show the expected behavior in resonance conditions: angles and displacements grow in time, as shown in Figure 22.

The second experiment is carried out with the goal of proving the mathematical accuracy of the developed model by substituting the time response values (appropriately derived where needed) into equation (34). The result, shown in Figure 23, ensures the identity between the left and right members of the equation, therefore validating all the calculations and models developed for the project. We must exclude the very first and last results in the graph, as they are errors produced by internal MATLAB functions in absence of following or preceding elements in the input vectors. This error check is performed in idle conditions.

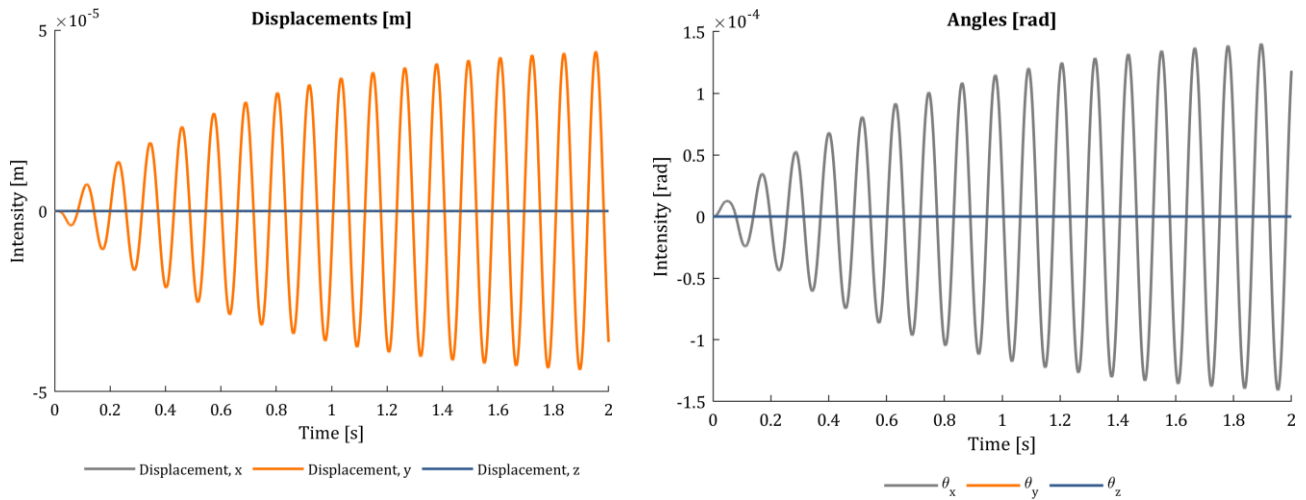


Figure 22 – Displacements and angles in resonance conditions

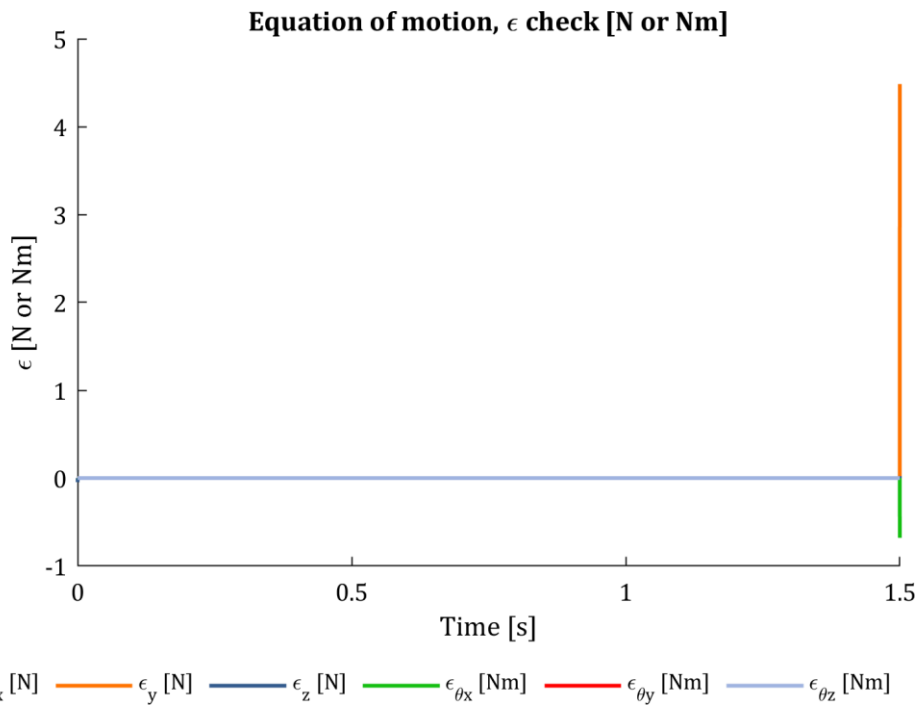


Figure 23 - Error check

5. Conclusions and final remarks

This study has been articulated in three phases: theoretical development, numerical implementation and simulation.

The first phase defined the mathematical models for both forcing input and system's motion, with the first making use of substitution masses and inertia moments in order to take into account every part of the crank and slider mechanism, and the second using a system of four triplets of springs and dampers to model the engine mounts. The forcing calculations were not approximated to any number of orders, in order to be able to determine the ones effectively present from the spectra of the forcing itself.

The second phase focused on reproducing said models in MATLAB, by creating a strongly OOP-based simulator, letting the user test any inline engine based on a set of given parameters. The result was a flexible, modular and reusable software which has been named P.I.E. Simulator. Particular attention was given to enabling the user to add defects to the ideal engine, under the form of weight tolerances for each piston, opening for simulations closer to the real case. A specific engine was chosen in order to gather data on which to perform simulation, with the choice falling onto a Toyota 2-JZ inline-six engine, of which CAD models were developed throughout the study.

Finally, in the third phase, six simulations were carried out: a first one was used to define the system's parameters, four were used to define the system's response to four different forcing inputs, and a sixth simulation was performed in order to investigate the effect of piston mass defects on the engine.

From the simulations, conclusions could finally be drawn. The engine forcing model has been verified by checking different types of inline engines against literature and finding consistent results. The system motion model was verified by checking the identity of the initial equation by substituting the data obtained from the simulations. With models having been validated, results show that inline-six engines are extremely balanced, with forces cancelling out up to the sixth order and leading to very limited displacements and rotations.

On the other hand, such an engine shows high sensitivity to manufacturing tolerances, which can increase forces up to two orders of magnitude, therefore requiring expensive processes to ensure the parts' quality needed for the engine to work as smoothly as its layout would allow.

Additionally, the nature of P.I.E. Simulator allows for wider future engine vibrations studies with minimal need for code changes.

6. References

- [1] Francesco Pellicano, Mechanical Vibration course notes, 2020
- [2] Nel, C.B. & Steyn, A.J. (2012). Stiffness and Damping Characterisation for a Hydraulic Engine Mount. Conference Proceedings of the Society for Experimental Mechanics Series. 6. 129-135. 10.1007/978-1-4614-2419-2_12.

Figures

Figure 1 - Simplified Model	4
Figure 2 - Calculation of the springs' displacements along the vertical axis	7
Figure 3 - Model for the inertial forces	8
Figure 4 – Forces transmitted to the chassis.....	15
Figure 5 - P.I.E. Simulator UML class diagram	18
Figure 6 - P.I.E. GUI.....	19
Figure 7 - 6-cylinder block CAD model.....	20
Figure 8 - Engine parts.....	21
Figure 9 - Mass and inertia tensor calculated by the CAD software.....	21
Figure 10 - Additional CAD models used to calculate parametric laws	22
Figure 11 - Piston dimensions in the minimum and maximum weight conditions	23
Figure 12 - Static measurements results	25
Figure 13 – Speed ramp simulation - time domain signals representation	27
Figure 14 - Speed ramp simulation - frequency domain signals representation.....	28
Figure 15 - Idle simulation - time domain signals representation	30
Figure 16 - Idle simulation - frequency domain signals representation	31
Figure 17 - Maximum power regime simulation - time domain signals representation ..	33
Figure 18 - Maximum power regime simulation - frequency domain signals representation ..	34
Figure 19 - Limiter simulation - time domain signals representation	36
Figure 20 - Limiter simulation - frequency domain signals representation	37
Figure 21 - Real piston mass defects simulation - forcing representation	38
Figure 22 – Displacements and angles in resonance conditions	40
Figure 23 - Error check	40

Tables

Table 1 - Engine specs and performance data	20
Table 2 - Engine properties empirical laws	22
Table 3 - Piston weights and dimensions	23
Table 4 - Stiffness and damping ratio data.....	24



Authors

Alexis Cariou
Lorenzo Clerici
Dario D'Orsi
Pietro Musso
Abdelhkim Nakiata
Giacomo Pirani
Matteo Raggi
Elia Zamperoni